AIAA

AIAA 95-2724

Effects of Slag Ejection on Solid Rocket Motor Performance

R. Harold Whitesides and David C. Purinton
ERC, Incorporated
Huntsville, AL

John E. Hengel and Stephen E. Skelley
NASA/Marshall Space Flight Center
Huntsville, AL

31st AIAA/ASME/SAE/ASEE
Joint Propulsion Conference and Exhibit
July 10-12, 1995/San Diego, CA

EFFECTS OF SLAG EJECTION ON SOLID ROCKET MOTOR PERFORMANCE

R. Harold Whitesides* and David C. Purinton**
ERC, Incorporated
Huntsville, Alabama

John E. Hengel*** and Stephen E. Skelley****
NASA Marshall Space Flight Center
Huntsville, Alabama

Abstract

In past firings of the Reusable Solid Rocket Motor (RSRM) both static test and flight motors have shown small pressure perturbations occurring primarily between 65 and 80 seconds. A joint NASA/Thiokol team investigation concluded that the cause of the pressure perturbations was the periodic ingestion and ejection of molten aluminum oxide slag from the cavity around the submerged nozzle nose which tends to trap and collect individual aluminum oxide droplets from the approach flow. The conclusions of the team were supported by numerous data and observations from special tests including high speed photographic films, real time radiography, plume calorimeters, accelerometers, strain gauges, nozzle TVC system force gauges, and motor pressure and thrust data. A simplistic slag ballistics model was formulated to relate a given pressure perturbation to a required slag quantity. Also, a cold flow model using air and water was developed to provide data on the relationship between the slag flow rate and the chamber pressure increase. Both the motor and the cold flow model exhibited low frequency oscillations in conjunction with periods of slag ejection. Motor and model frequencies were related to scaling parameters. The data indicate that there is a periodicity to the slag entrainment and ejection phenomena which is possibly related to organized oscillations from instabilities in the dividing streamline shear layer which impinges on the underneath surface of the nozzle.

---

* Manager, Propulsion; AIAA Associate Fellow
** Engineer, Propulsion Analysis Group
*** Senior Aerospace Engineer, ED34
**** Aerospace Engineer, ED34

Introduction

Space Shuttle Mission STS-54, launched 13 January 1993, experienced a short duration pressure deviation in the right-hand Reusable Solid Rocket Motor (RSRM-29B) of 13.9 psi at 67.5 seconds into the burn. Pressure perturbations and some roughness of the pressure trace have been general characteristics of RSRM's with previous occurrences approaching the magnitude of RSRM-29B; however, this incident resulted in the largest vehicle thrust imbalance calculated to date. A joint NASA/Marshall Space Flight Center and Thiokol team was assembled to conduct an in-depth investigation of the exact cause of the pressure perturbations and to determine the limiting case. After extensive analyses and testing, including specially instrumented full scale motor static tests, the joint MSFC/Thiokol team concluded that the source of the pressure perturbations was the periodic ingestion and discharge of molten aluminum oxide slag from the reservoir around the submerged nozzle nose which serves to trap and collect individual aluminum droplets from the approach flow. A similar phenomena has been observed in other large solid rocket boosters with aluminized composite propellants and submerged nose nozzles. The conclusions of the investigation group were supported by numerous observations and data including flight and static motor high speed photographic films, static motor Real Time Radiography, chamber pressure and thrust data, plume calorimeter data, nozzle accelerometer data, case and nozzle strain data, and nozzle TVC system force data and more.

Objectives

A combined analytical and experimental approach was adopted to develop an understanding of the effects of slag ejection on motor performance. A simplistic quasi-steady analytical model was formulated for the purpose

of determining the instantaneous slag flow rate and the total quantity of slag required to produce a given pressure perturbation. The analytical model of the ejection of a stream of slag was also used to evaluate the relationship between thrust and pressure during the slag ejection event. The analytical model was supported by comparison with static motor test results and cold flow model data. The objectives of the cold flow model tests were to demonstrate that simulated slag ejection through a rocket motor nozzle will produce an increase in chamber pressure and to obtain quantitative measurements of the amplitude of the pressure increase relative to the simulated slag flow rate. This data could be related to the full scale motor through the application of appropriate scaling parameters and used to calibrate the analytical slag ballistics model. A secondary objective of the cold flow tests was to investigate potential internal motor triggering mechanisms for slag ejection. The triggering mechanism is defined to be the causal factor in the process of sudden and periodic entrainment of slag from the reservoir underneath the nozzle into the gas flow and subsequent expulsion through the nozzle.

Slag Ballistics Model

Model

An analytical slag ballistics model was conceived to determine the quantity of expelled slag associated with a given pressure perturbation. Since the time duration of the rise time of a pressure perturbation was long (~0.8 sec.) compared to the acoustic wave travel time in the motor (0.03 sec.) a quasi-steady approach was utilized to develop the model. The model is based on the concept of calculating a time-dependent quasi-steady slag flow rate through the nozzle throat from the continuity equation. The velocity of the slag is computed from a trajectory analysis of a hypothetical sphere of slag as it flies through the nozzle. The slag stream is treated as a continuous parade of spheres. The cross sectional flow area of the stream or the sphere diameter is calculated from a transient calculation of the amount of throat area blockage required to produce a given pressure increase. The slag is assumed to be a slurry mixture of molten aluminum oxide and combustion gases and has a density of "K" times the density of aluminum oxide at combustion temperature where K is approximately 0.2. The instantaneous slag flow rate is calculated for time steps spanning the entire period of apparent nozzle blockage and

integrated to determine the total slag quantity discharged.

The analysis steps and equations utilized are as follows for a given motor pressure perturbation. The differential form of the continuity equation is solved for the effective throat area as a function of time.

$$\frac{dm_g}{dt} = \frac{dm_D}{dt} + \frac{\left\{P_c\left(\frac{dV}{dt}\right) + V\left(\frac{dP}{dt}\right)\right\}}{RT} \quad (1)$$

where

$$\frac{dm_g}{dt} = \rho_p \cdot r_b \cdot A_s \quad \text{(Mass Generation)} \quad (2)$$

and

$$\frac{dm_D}{dt} = \frac{A_t \cdot P_c}{C^*} \quad \text{(Mass Discharge)} \quad (3)$$

The motor surface area, burn rate and other ballistic parameters are used to calculate an effective throat area versus time during the pressure perturbation. The throat area blockage is then calculated by subtracting the effective throat area from the nominal throat area without blockage at the appropriate times.

$$A_{block} = A_{t_{nominal}} - A_{t_{effective}} \quad (4)$$

The next step is a trajectory calculation of a single sphere in an assumed parade of spheres as they fly through the nozzle. The sphere diameter is determined by setting the frontal area of the sphere to the throat blockage. The flowfield through the nozzle is calculated from the one-dimensional, compressible, isentropic flow equations. The velocity of the slag sphere at a specific time step is given by

$$V_{slag(t+\Delta t)} = \left\{\left(G_F + \frac{F_D}{M_s}\right)2\Delta L + V_{slag(t)}^2\right\}^{\frac{1}{2}} \quad (5)$$

where G_F = Vehicle acceleration
       F_D = Drag force on slag sphere
       M_s = Mass of slag sphere
       ΔL = Distance traveled, incremental

The drag force is based on the differential between the slag velocity and the gas velocity and a drag coefficient of 0.5. The mass of the slag sphere is based on a diameter from the throat

area blockage and a density for the slag slurry calculated from the density of molten aluminum oxide (110 lbm/ft^3) multiplied by a factor, K. The value of "K" is set to 0.20 based on a correlation of the cold flow model data.

Once the slag slurry velocity profile through the nozzle is calculated, the slag flow rate at the throat plane is calculated by applying the continuity equation at each time step.

$$\dot{m}_s = \rho_s \cdot A_{block} \cdot V_{slag_{throat}} \qquad (6)$$

The total slag weight discharged during a pressure perturbation is then determined by integrating the above equation over the time interval of nozzle blockage. Also, the total thrust is calculated by adding the slag momentum at the nozzle exit plane to the gas thrust.

$$F_{total} = F_{gas} + F_{slag} \qquad (7)$$

where

$$F_{gas} = P_c \cdot A_{t_{effective}} \cdot C_{FM} \qquad (8)$$

and

$$F_{slag} = \dot{m}_s \cdot V_{slag_{exit}} \qquad (9)$$

The thrust to pressure ratio is then calculated by

$$\frac{F}{P} = \frac{F_{total}}{P_c} \qquad (10)$$

Increases in thrust to pressure ratio are predicted for certain quasi-steady slag ejection events which are primarily attributed to the thrust increase associated with the slag momentum term. This result is consistent with Murdock's study[1] of thrust perturbations from single and multiple bodies passing through a solid rocket nozzle. He found that the total impulse from a mass ejection event is always positive.

Results

This simplistic, analytical model was used to model the pressure perturbation in RSRM-29B for the STS-54 flight. This motor exhibited a pressure perturbation of 13.9 psi at approximately 67 seconds. The motor pressure and model results are shown in Figure 1. The calculated pressure during blowdown after the nozzle is unblocked goes below the motor data due to the use of a constant burn surface. The major output of the analysis is the calculated nozzle throat blockage as a function of time which is also shown

in Figure 1. The slag flow rate calculated by the model during the 0.8 seconds of nozzle blockage is shown in Figure 2. The integrated slag weight is 1446 lbm. Parametric calculations were performed with the model to determine the variation of slag weight and the thrust enhancement factor with pressure perturbation amplitude. Results are plotted in Figure 3. The pressure perturbations were assumed to occur in the same 0.8 second time period. The thrust enhancement is the thrust increase with slag flow divided by the thrust increase without slag flow for a given pressure perturbation. It may also be stated as the percent change in thrust divided by the percent change in pressure during a slag induced pressure perturbation. The values above unity are due to the momentum effects of slag ejection which appear to be more significant at the lower pressure amplitudes. Without the slag momentum effect, the throat area reduction reduces the thrust to pressure ratio which would result in a thrust enhancement value less than unity. The thrust enhancement value during a 9 psi pressure perturbation for static motor test QM1 was calculated directly from measured thrust and pressure data to be 1.3 which required a slag density factor of 0.3 to agree with model results as shown in Figure 4. The cold flow model simulation using water yielded a "K" value of 0.2
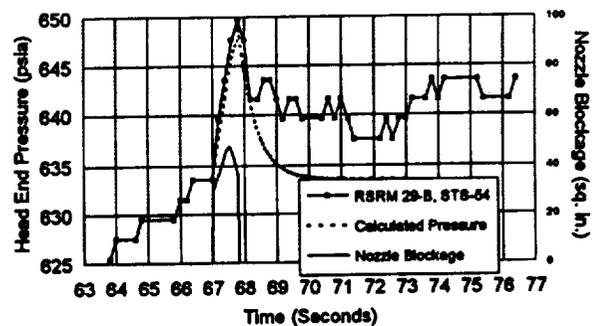

Figure 1. Nozzle Blockage Analysis
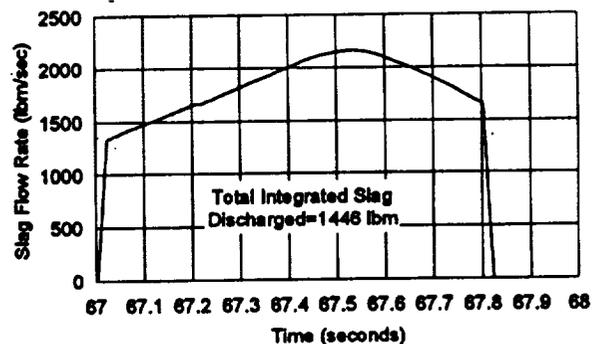
Figure 2. RSRM 29-B, STS-54 Slag Flowrate

American Institute of Aeronautics and Astronautics

which was used to generate a set of model predictions also shown in Figure 4. Although high accuracy in predicting the thrust enhancement ratio is not claimed for the model, the apparent agreement between motor data and model results supports the realism of thrust enhancement values greater than unity.
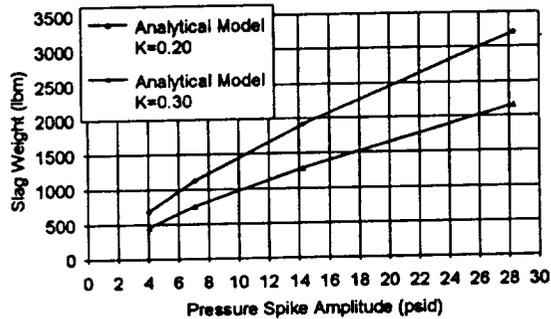

Figure 3. Predicted Slag Weights
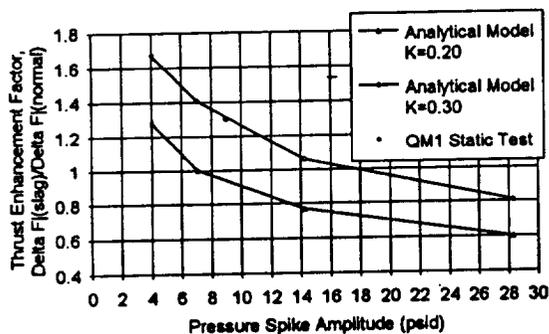
Figure 4. Thrust Enhancement Factor

Cold Flow Slag Model

Model Description

A simulation of the effects of slag ejection on motor performance were achieved using a scaled air flow model with water to simulate slag. An existing horizontal bed solid rocket motor air flow test facility and model chamber hardware were adapted to the desired test configuration. A 6.5 percent scaled RSRM nozzle with submerged nose and the full length contoured expansion section was designed with fixed gimbal angles of 0, 2, and 4 degrees. The chamber to throat contraction ratio simulates a motor burn time of 67 seconds when slag ejection is active. Water injection ports were provided underneath the nozzle nose in the aft end of the cavity to enable flooding the cavity with water at low velocities. This would provide a pool of simulated slag to be

naturally entrained by the air flow and expelled through the nozzle in a manner to simulate a horizontal static motor firing. The model was also provided with a centerline axial fluid injector to enable data comparison with an earlier precursor model with a converging diverging 10 percent scale nozzle and centerline water injection. A sketch of the model is provided in Figure 5. The dashed line near the wall represents the scaled position of the burn surface at 67 seconds. The model walls are nonporous and all flow is supplied down the bore of the model. The first joint upstream of the nozzle represents the aft field joint including the inhibitor. A photograph of the installed model and water injection system is shown in Figure 6. The model is disconnected from the exhaust diffuser and the view is looking upstream. A portion of the nozzle exit is visible along with the model chamber and the forward plenum into which four facility air supply pipes deliver the total model flow. Each of the four facility supply pipes includes a choked metering nozzle to prevent model chamber pressure excursions related to slag ejection from affecting the mass flow rate of air through the model. The stainless water supply tubing is routed to each of 12 remote operated valves positioned circumferentially around the model adjacent to each injection port located in the aft end of the chamber cavity underneath the nozzle nose. The large lines and ports are designed to minimize the water injection velocity. Water is delivered to the model from a pressurized tank through a metering orifice and controlled by remote operating valves.

The RSRM 6.5 percent Scaled Slag Ejection Model was tested in the Marshall Space Flight Center Solid Rocket Motor Air Flow Facility (SAF).[2] This facility has the capability to test a 10 percent scale RSRM at full scale Reynolds number. The facility is a pressure blowdown system with a tank storage capacity of 9100 cubic feet at 1960 psia. A flow rate of up to 320 lbm/sec can be delivered to the model at pressures to 1200 psia. The delivered air is filtered and passed through a calibrated venturi for metering. The model inlet pressure is controlled by a quiet trim control valve with an automated feedback control system. The mass flow through the system is exhausted to the atmosphere through the diffuser, an exhaust pipe, and then a vertical 85dB silencer. The diffuser enables the test model to operate at the full scale booster nozzle expansion ratio without flow separation. For air, this results in exit plane pressures down to 3 psi.

THROAT PLANE
STA 1845.907 RSRM

22.937

PIVOT POINT

R 4.260

R 4.863

PROPELLANT SURFACE AT
67 SECONDS BURN TIME

EXISTING SPOOL PIECE

INHIBITOR SIMULATOR

CAVITY FLUID
INJECTION PORT

AFT END OF PROPELLANT

DIFFUSER DUCT

RSRM SCALED NOZZLE

AXIAL FLUID INJECTOR
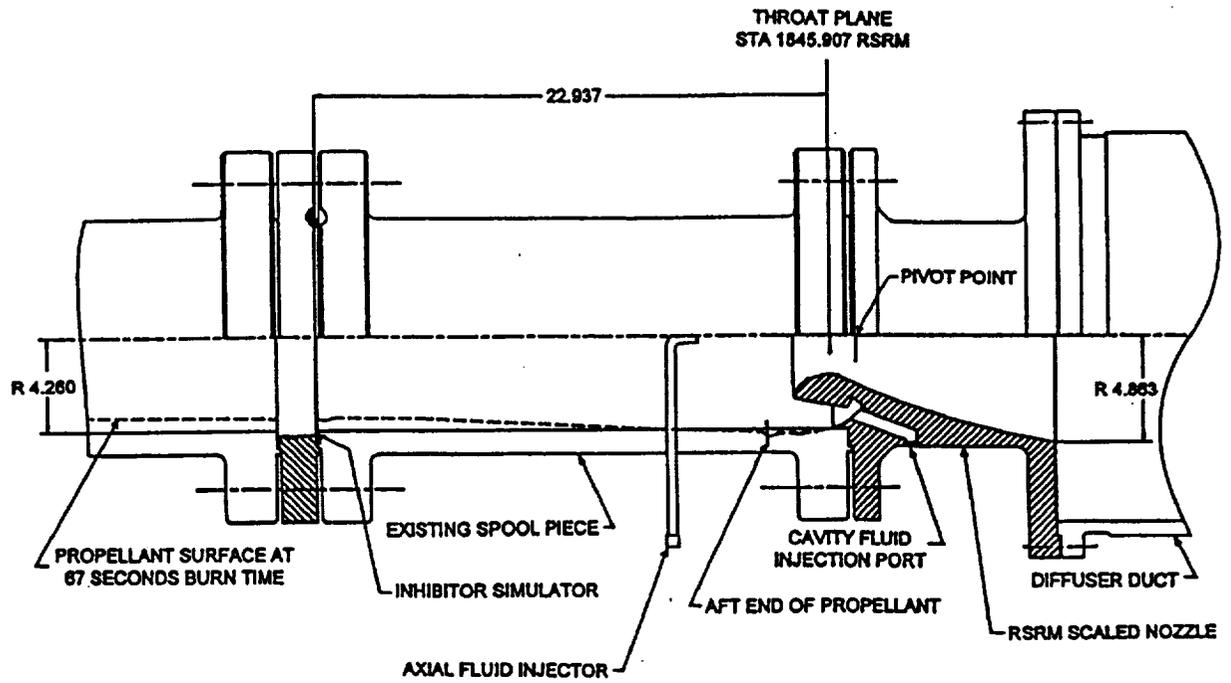
Figure 5. RSRM 6.5% Scaled Slag Ejection Model
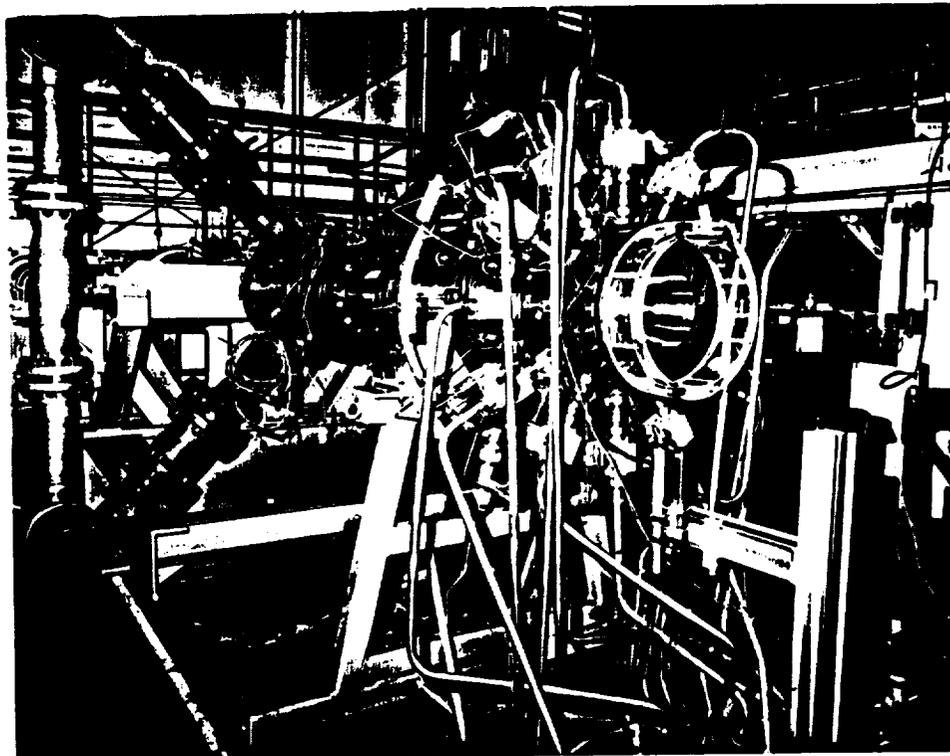
Figure 6. Cold Flow Slag Ejection Model and Facility

The cold flow slag model was instrumented with total pressure and temperature probes, static pressure taps and dynamic pressure gauges. Pressure data was measured using differential pressure transducer modules as part of a 256 channel electronic scanning data recording system. The data is recorded, stored, and converted to engineering units on a Hewlett-Packard computer. In addition, a miniature video system and camera in the model chamber was used to observe the fluid activity around the nozzle nose during the ejection event.

In order for the subscale cold flow slag ejection model results to be applicable to the full scale RSRM, it is important to employ certain scaling parameters in the design of the model and the selection of operating conditions. The most straight forward scaling parameter to satisfy is the air flow Reynold's Number. This will assure similarity in the structure of the highly turbulent flowfield. The model Reynold's Number is matched to the full scale motor value of 40.8E06 at the throat by proper selection of the model operating chamber pressure. The Weber Number (ratio of surface tension forces to dynamic forces) was matched within 42 percent to attempt to replicate behavior of the entrained droplets in the flowfield. Properties of air and water were used in the model and properties of molten aluminum oxide and combustion gases in the motor. The match between the fluid droplet to gas flow momentum ratio was also calculated. Lastly, the nominal water injection flow rate to the model was calculated to provide the same percent blockage of the nozzle throat area as experienced in the full scale RSRM 29-B. This nozzle throat blockage is approximately 2 percent and the slag ballistics model was used to calculate the required water flow rate.

Test Results and Correlation

The model test conditions were varied about nominals to investigate the effect of the controlled parameters on the test results. Operating test conditions and summary results are tabulated in Table I for representative runs. The pressure increase listed is the time-averaged shift in model chamber pressure experienced during the period of water injection. The frequency and dynamic amplitude results will be discussed in a later section. Test results for a representative run, number 99-0, are shown in Figure 7 at a data rate of 100 samples per second. The upper portion shows the raw test data for the run while the lower

portion shows the data after a 100 point moving average was performed. The sudden start transient and the overshoot in both chamber pressure and water flow rate, as calculated from the orifice pressure differential, is readily apparent. However, as the mean water flow rate settles out, the chamber pressure maintains a mean offset from the value before water flow. The DC values for the chamber pressure increase and water flow rate are determined from the 100 point moving average plotted in the lower portion of Figure 7.
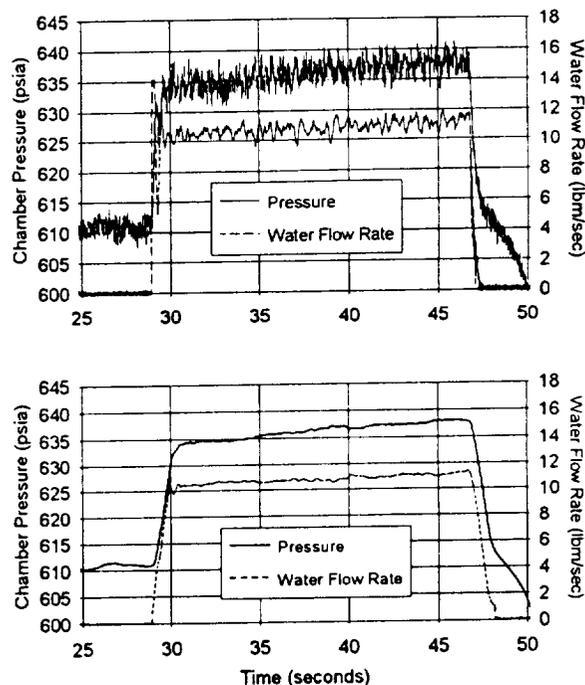

Figure 7. Cold Flow Model Test Data

The DC values for the chamber pressure increase are plotted against the water flow rate in Figure 8. The slag ballistics model was applied to the cold flow nozzle flowfield using air and water properties to calculate chamber pressure increases over a similar range of water flow rates where the "K" value was adjusted to minimize the square root of the sum of the squares for the deviations between data and model predictions. The resulting value of "K" is 0.20 and the calibrated slag ballistics model prediction is represented by the solid line. The "K" value of 0.20 represents the mass fraction of water in the entrained "slurry" mixture of air and water. The data could obviously be somewhat better represented by a linear regression fit; however, the slag ballistics model correlation is based on a physical, mechanical model which provides the means to apply the cold flow data to

Table I. Experimental Data from RSRM Scaled Slag Ejection Model

Run No.	Chamber Pressure, psia	Water Flow Rate, lbm/sec	Gimbal Angle, Degrees	Pressure Increase, psid	Lowest Frequency, Hertz	Amplitude, RMS psi
98-0	619	0.83	0	2.30	1.56	0.110
97-0	621	4.89	0	12.73	1.95	0.258
99-0	611	10.72	0	25.36	2.73	0.279
102-0	301	2.47	0	6.50	1.56	0.172
101-0	303	7.62	0	15.33	2.34	0.222
53-0	625	0.95	4	7.15	1.56	0.111
51-0	626	3.60	4	11.92	2.34	0.123
52-0	628	5.30	4	15.45	2.73	0.131
44-0	470	1.40	4	5.15	1.95	0.176
45-0	468	8.46	4	20.73	2.73	0.147
49-0	313	7.50	4	16.38	1.56	0.272
48-0	313	10.93	4	21.90	3.12	0.152
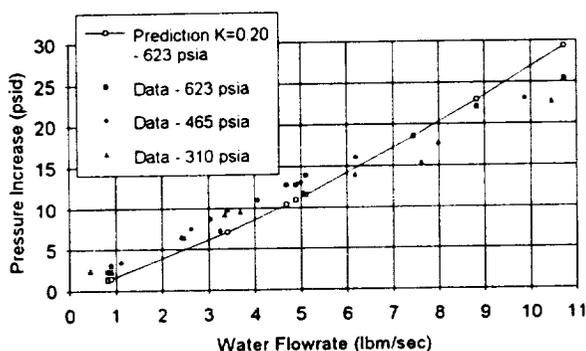
Figure 8. Cold Flow Model Data Correlation

the full scale by switching to the motor nozzle flowfield and using combustion gas and molten aluminum oxide properties.

Motor and Model Low Frequency Oscillations

Motor Observations

The pressure perturbation investigation for flight STS-54 revealed that pressure perturbations for a number of both static and flight motors tend to occur at a frequency of approximately 0.6 Hertz. The shapes and magnitude of the pressure perturbations are similar between static and flight motors and the time of highest activity (68-72 seconds) is similar although the time of initial activity is several seconds earlier for static motors. Nozzle vectoring can induce strong pressure perturbations traceable to slag ejection but pressure perturbations also occur without any nozzle vectoring on static test motors.

TEM-10 was the first static test motor instrumented for detection of slag accumulation and ejection as it relates to pressure perturbations. The special additional instrumentation included real time radiography (RTR), plume calorimeters, and nozzle accelerometers. The nozzle was not vectored for this test which makes the results more relevant to the cold flow tests and for studying the relationships between slag ejection and low frequency oscillations. Nozzle vectoring is known from other tests to be capable of causing large slag ejection events depending on the timing, magnitude, and direction of the nozzle movement. An overall pressure trace is shown in Figure 9. The roughness in the pressure trace beginning just before 60 seconds is evident along with a small pressure blip at approximately 69 seconds. A PSD isoplot of the spectral analysis is
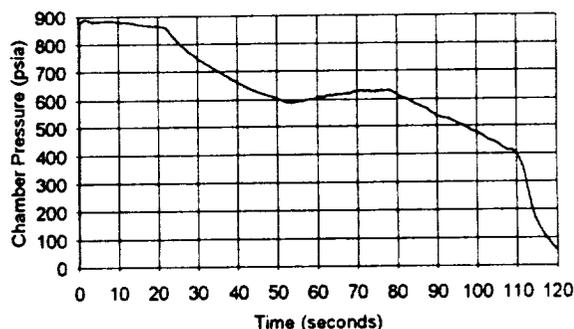

Figure 9. TEM-10 Chamber Pressure Data

shown in Figure 10. The first longitudinal mode at 15 Hertz is visible on the right of the figure. Also, a very low frequency oscillation in the 0.5 to 3.0 Hertz range commences at about 54 seconds and

continues until about 80 seconds. It diminishes then rebuilds until motor web time. These low frequency oscillations have been observed at the same time spans in numerous static and flight motors. The build in amplitude of these low frequency oscillations appears to be associated with slag ejection although there are "ballistic" frequencies present in the data at very low values. "Ballistic" frequencies result from undulations in the pressure trace caused by sudden changes in propellant burn surface area from geometric effects such as burning across a thickened case insulation zone over a factory joint. These frequencies are at very low values of 0.1 to 0.2 Hertz. They do not appear to be the explanation for the frequencies observed between 0.5 and 3 Hertz.
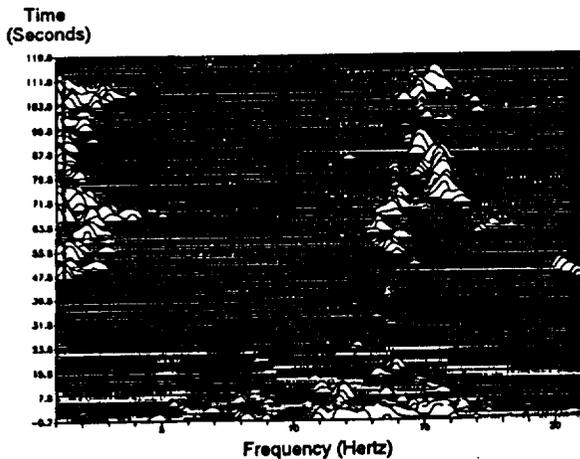
Figure 10. TEM-10 Dynamic Chamber Pressure

RTR film shows that at about 40 seconds slag begins collecting under the nozzle nose cavity although the propellant is not completely consumed under the nose until about 65 seconds. A spectral analysis of the motion of the slag underneath the nozzle nose, as measured from film density gradients, also indicates a low frequency activity beginning at approximately 55 seconds and increasing in magnitude with burn time. Figure 11 shows the frequency range of the slag motion to be primarily in the 0.5 to 3 Hertz range. Calorimeter data for plume radiation shown in Figure 12 also exhibits low frequency oscillations up to 3 Hertz beginning about 55 seconds and building in amplitude during the period associated with slag ejection.

A power spectral density calculation was performed for the dynamic head end pressure

data and the results are shown in Figure 13. The two lines correspond to a time period of 19.8 seconds to 40.6 seconds, when no slag is being ejected, and a time period of 50.2 to 78.2 seconds which includes slag ejection. A significant increase in energy between 0.5 and 3 Hertz is evident during the period of slag ejection. The largest gain is at the lowest plotted frequency of 0.5 Hertz. Lower frequencies are not plotted to eliminate the contribution of "ballistic" frequencies in the results.
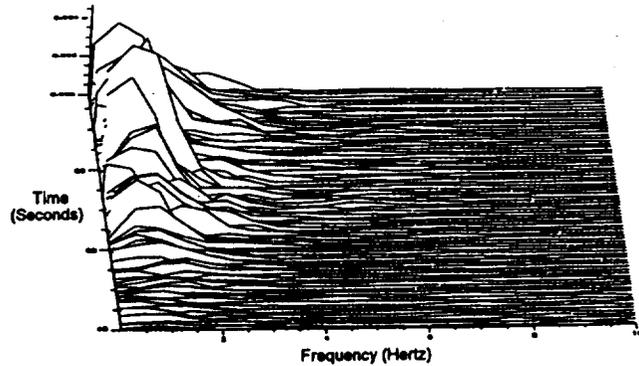

Figure 11. TEM-10 Real Time Radiography Data
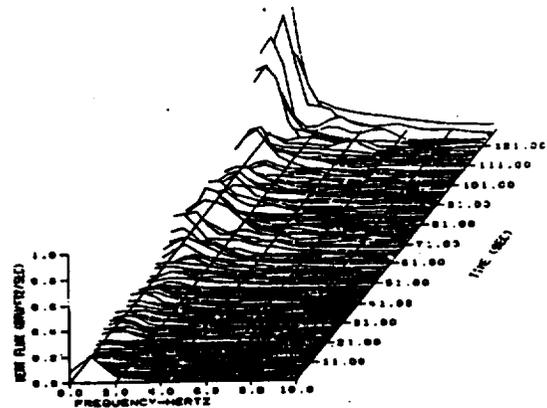
Fig. 12. TEM-10 Dynamic Plume Heat Flux Data
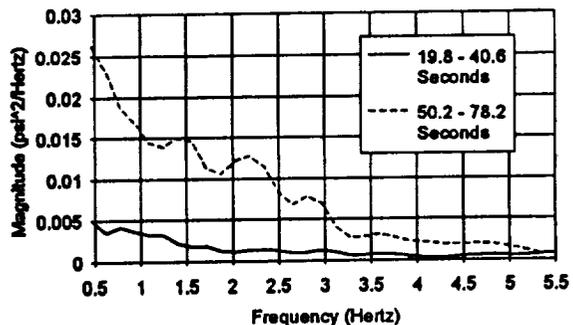
Figure 13. TEM-10 Chamber Pressure PSD

Figure 14 shows the corresponding significant percentage increase in amplitude of the dynamic pressure oscillations (between frequencies of 0.5 to 5.5 Hertz) that occurs beginning at approximately 55 seconds. (Six seconds must be added to plot scale values due to length of sample period in analysis.) The bottom portion of Figure 14 shows that the low frequency oscillations are present in the motor before the period of slag ejection implying that the basic periodic gas dynamic phenomena is always present and significant amplitude increases result when the phenomena interacts with slag ejection.
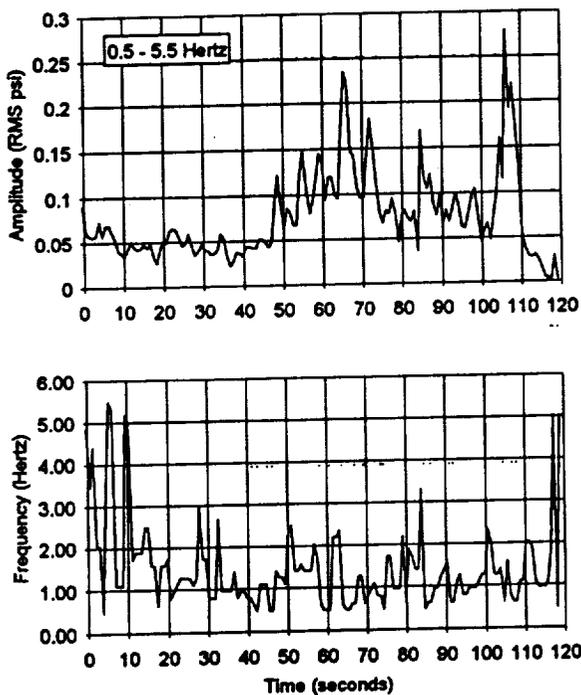
Figure 14. TEM-10 Dynamic Chamber Pressure

Thus the periodicity of slag entrainment and ejection though the nozzle is supported by numerous observations associated with static and flight motors. The Real Time Radiography film shows the formation of a slag reservoir underneath the nozzle nose during the later half of the motor burn time which undoubtedly is formed from a collection of individual "droplets" which have impacted the underneath side of the nozzle and/or the aft case dome. This observation is consistent with other large motors with composite aluminized propellants. Furthermore, the slag reservoir appears to be severely and periodically disturbed and churned up by the gas flow into a "slurry" or mixture of slag and gas. The motion of this slurry mixture is driven by the large scale

turbulent eddies associated with the separated flow underneath the nozzle nose and the asymmetries of the aft case region caused by both nozzle gimballing and the presence of the slag reservoir itself. The dynamic pressure of the gas flow approaching the nozzle is very high at 3.5 psi and capable of exerting high forces and accelerations on the order of one-hundred g's on the slag globules. These turbulent gas dynamic forces result in slag being entrained and expelled through the nozzle before the slag reservoir fills to the level of the nose tip. Thus the submerged nozzle nose cavity becomes "aerodynamically full" before it becomes "geometrically full". The entrainment and expulsion of the slag is naturally periodic because of the large scale turbulence existing in the aft dome region of the submerged nozzle motor.

The shear layer formed by the dividing streamline between the flow entering the nozzle and the stationary, recirculating vortex of the separated flow underneath the nozzle nose is the prime suspected source of the periodic turbulent disturbances. Instability induced excitation sources are frequently associated with flows which include the presence of shear layers. Shear layers which impinge on surfaces or edges are particularly prone to generating instabilities. The impingement of a disturbance in a shear layer on a downstream surface provides an upstream feedback mechanism which can lead to organized oscillations of the shear layer.[3] The shear layer associated with the dividing streamline underneath the RSRM nozzle nose does, in fact, impinge on the underneath surface of the nozzle nose as shown in Figure 15. This result is from a steady state CFD solution of the RSRM aft end flowfield at a burn time of 67 seconds.
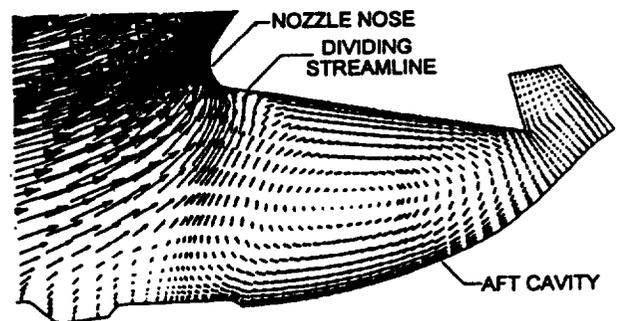

Figure 15. Dividing Streamline Plot

The structure of the mean flow field in the aft nozzle cavity of a 7.5 percent scale air flow

model of the RSRM was measured and photographs of surface oil flow patterns were recorded in the NASA/Marshall Space Flight Center Solid Rocket Motor Air Flow Facility.[4] Test configurations included various burn times and nozzle gimbal angles up to 7 degrees. Complex three-dimensional flows were recorded with extreme sensitivity of circumferential velocities to small gimbal angles. Intense vortical flows and extreme sensitivity of circumferential pressure distribution to small gimbal angles was also noted by Waesche and Marchman in water and air models of the Space Shuttle booster motor configuration.[5] Earlier water flow visualization tests were conducted with a 1/8th scale model of the submerged nozzle nose zone of the Space Shuttle Booster Motor by Waesche, et al. in a facility at Virginia Polytechnic Institute.[6] The observation of injected dye flow patterns revealed the presence of vortices which periodically formed between the nozzle inlet and the aft dome wall in the shear layer zone. These vortices started at the motor case wall and trailed into the nozzle inlet. The aft dome cavity was periodically "flushed" by these vortices which caused a circumferential flow around the dome toward the vortex until it dissipated and another was formed. Figure 16, an enhancement of Figure 7 in Reference 6, depicts these vortical flows in the aft dome. When the nozzle was gimbaled, formation of vortices including multiple vortices was enhanced, primarily at the point of closest proximity of the nozzle nose to the motor case wall. The authors of Reference 6 further stated that the flow carried into the nozzle by the vortices could displace the core flow and possibly cause chamber pressure pulses. The phenomena of inlet-vortices has been observed between jet
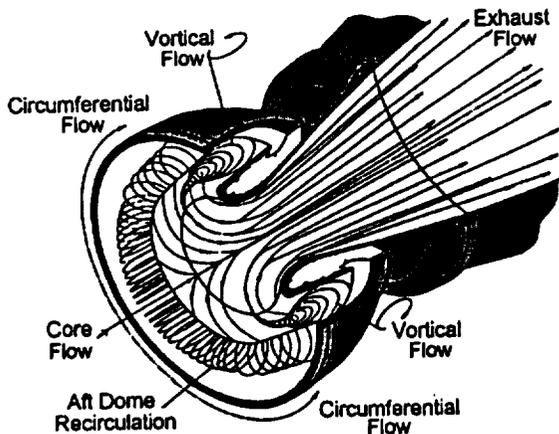
engine inlets and a nearby ground plane. Mechanisms causing the formation of inlet-vortices include shear layers from an upstream location and cross flows over the inlet. An experimental and theoretical treatment of this topic is available in Reference 7.

Model Observations

The frequency of the periodic motion of the slag in the aft cavity around the nozzle nose must be related to the local gas velocities and a length scale dimension associated with the dividing streamline shear layer within the aft cavity region. Such frequencies would be expected to be much less than motor acoustic frequencies. Assume that the frequency of the coherent shear layer induced oscillation can be represented by the equation:

$$\frac{f}{n} = \left(\frac{V_c}{L_c}\right) = \left(\frac{M_c \cdot C}{L_c}\right) \quad (11)$$

where f = frequency
  n = stage of oscillation
  V_c = characteristic velocity
  M_c = characteristic Mach number
  C = local sonic velocity
and L_c = characteristic length scale.

Then

$$\frac{f_{model}}{f_{motor}} = \frac{C_{model}}{C_{motor}} \cdot \frac{L_{motor}}{L_{model}} = \frac{1107}{3495} \cdot \frac{1}{0.065} \quad (12)$$

and

$$\frac{f_{model}}{f_{motor}} = 4.87$$

Therefore, for a motor turbulence low frequency range of 0.5 to 2.2 Hertz, the expected range for the cold flow model would be 2.4 to 10.7 Hertz. The spectral frequency analysis results for the cold flow model data show this corresponds closely with the measured range of the low frequency oscillations in the model. Figure 17 is a PSD isoplot of the model chamber pressure which shows the onset of low frequency oscillations in a low frequency range of up to approximately 10 Hertz. The first longitudinal mode of the model is 61 Hertz, well above the observed low frequency range. The oscillations begin with initiation of water flow and continue until the end of the test as does the water flow. The small amount of activity

Figure 16. Aft Dome Flow Patterns (Ref. 6)

at the beginning of the run is due to a residual water pool in the model chamber from leaking water shut-off valves. Figure 18 is a PSD isoplot of the nozzle exit plane wall pressure which shows the same frequency range at the same time as the chamber pressure. This signature is caused by the expelled fluid stream passing through the nozzle at subsonic speeds thus generating shock waves which pass over the surface of the nozzle and the face of the dynamic pressure transducer.

Time
(Seconds)
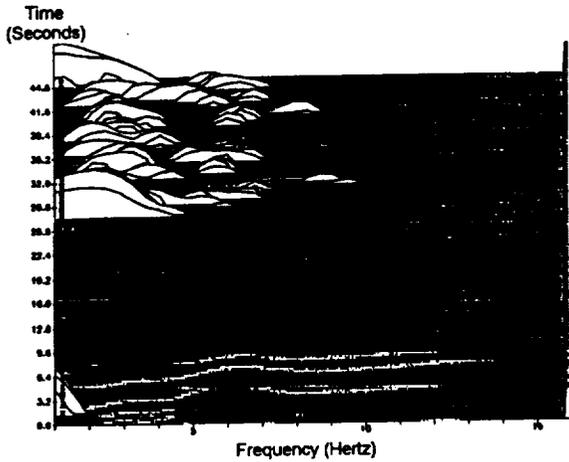
Frequency (Hertz)

Figure 17. Model Dynamic Chamber Pressure

Time
(Seconds)
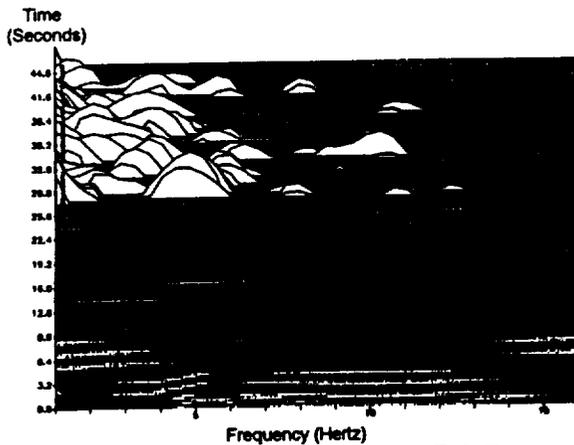
Frequency (Hertz)

Figure 18. Model Dynamic Nozzle Exit Pressure

The significant increase in energy level during the period of water injection at frequencies under 10 Hertz is readily apparent in the Figure 19 PSD plot which shows the peak magnitudes to be between 2 to 3 Hertz. The amplitude and frequency of model chamber pressure oscillations are shown for the entire test period in Figure 20. The top portion of the figure shows the overshoot spike of the start-up transient and higher amplitude during the period of water injection.

The lower portion of the figure shows the frequency range of 2 to 10 Hertz is active before water injection is initiated but at much lower amplitudes. Thus the turbulent instability has a periodicity that is present before and independent of the water entrainment and injection phenomena. The process of water injection merely increases the amplitude of oscillations already present.
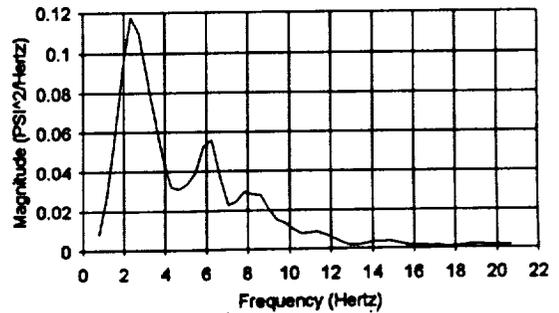

Figure 19. Model Chamber Pressure PSD
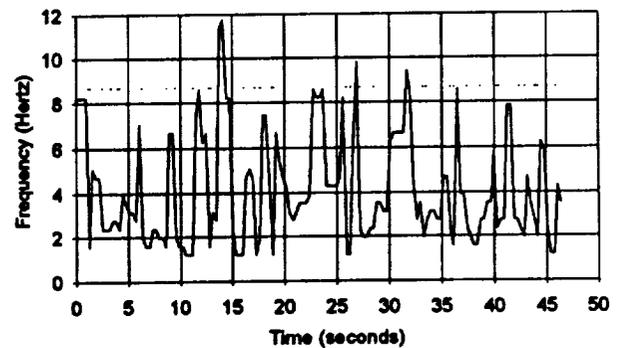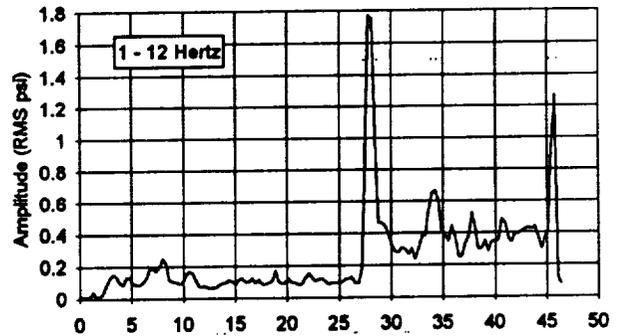
Figure 20. Model Chamber Pressure
Amplitude and Frequency

The same information is presented in Figure 21 for the nozzle exit plane wall pressure. The amplitude plot in the top portion of the figure shows the sudden increase to values over an order of magnitude higher than the amplitude of

chamber pressure oscillations during water injection. Thus the nozzle wall pressures are not merely following the chamber pressure oscillations through propagation of pressure waves but are the result of strong shock waves from the subsonic water particle stream being ejected through the nozzle. The frequency plot in the lower half of the figure shows that the water injection is periodic in nature with a frequency range from 2 to 10 Hertz matching the frequency range of the chamber pressure oscillations. Therefore the increase in amplitude of chamber pressure oscillations during water injection must be due to the nozzle blockage effect of simulated slag ejection rather than some other unexplained cause. The nozzle wall frequency data before . water injection is dominated by a data recording artifact and is not meaningful.
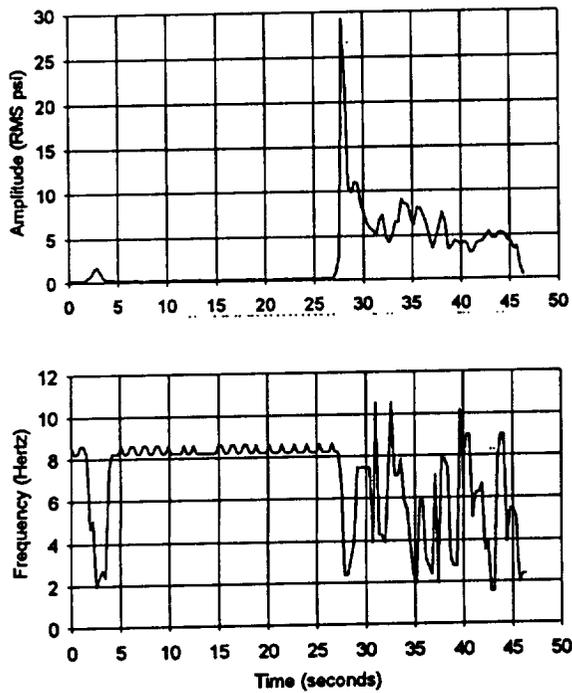

Figure 21. Model Nozzle Exit Pressure Amplitude and Frequency

The amplitude of the chamber pressure oscillations at the first stage frequency is plotted against water flow rate in Figure 22 for two nozzle gimbal angles of 0 and 4 degrees. The 4 degree nozzle gimbal angle is for movement of the nozzle nose downward toward the water pool. The amplitude is seen to increase with water flow rate with the 0 degree gimbal angle resulting in the highest amplitudes. The 4 degree gimbal angle probably allows less water to accumulate since

entrainment would occur more readily with the nose down. Less water accumulation would mean less water available for the periodic ingestion cycles. The first stage frequency changes with water injection rate are shown in Figure 23. Higher water injection rates may result in more filling of the aft dome cavity under the nozzle nose thereby decreasing effective cavity dimensions and possibly length scales which would increase the frequency of the shear layer induced instability.
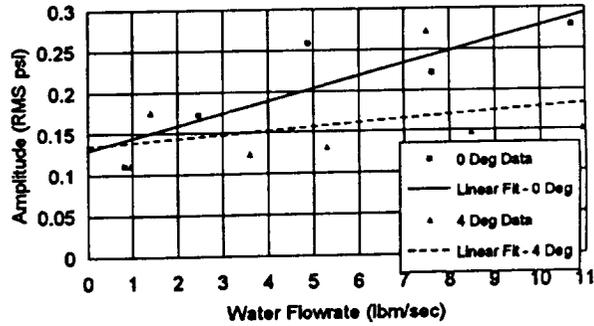

Figure 22. Model Chamber Pressure Amplitude
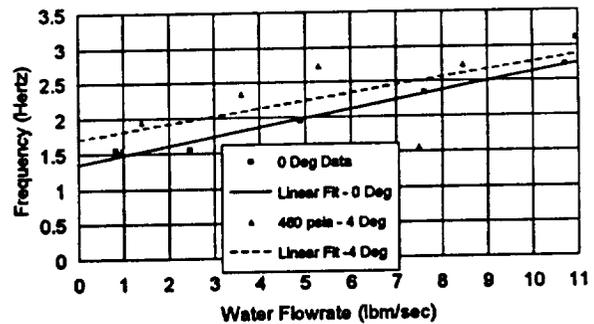
Figure 23. Model Chamber Pressure Frequencies

Conclusions

(1) A slag ballistics model to relate pressure perturbation magnitude to slag quantities was developed and shown to be consistent with cold flow model data and static motor test data.

(2) The ejection of a continuous stream of slag can result in an enhanced thrust to pressure ratio for certain conditions as evidenced by the slag ballistics model and motor test data.

(3) A cold flow model was successfully developed and used to generate data for relating chamber pressure increases to water simulated slag flow rate.

(4) The RSRM firing data shows increased activity at low frequencies (0.5 to 3 Hertz) during times of slag expulsion which is evidence of the role of turbulent shear layer induced instabilities in the entrainment and ejection of slag.

(5) Dynamic pressure data for the scaled RSRM cold flow model also reveals the presence of low frequency oscillations which can be directly related to the motor low frequency oscillations through appropriate scaling considerations.

(6) The cold flow model dynamic pressure data show that the amplification of the low frequency oscillations during water flow is directly traceable to the periodic entrainment of water from the cavity under the nozzle nose and the discharge of this water through the nozzle.

(7) The first stage frequency and amplitude of the model low frequency oscillations increases with simulated slag flow rate. A nose down gimbal angle of 4 degrees decreases the oscillation amplitude.

Acknowledgments

References

1. Murdock, John W., "Rocket Thrust Perturbation from Discharge of an Inert Body," Journal of Propulsion and Power, Vol. 2, No. 2, March - April 1986.

2. Bacchus, D. L., O. E. Hill and R. H. Whitesides, "Facility For Cold Flow Testing of Solid Rocket Motor Models," 1992 JANNAF Propulsion Meeting, Indianapolis, Indiana, 24-27 Feb. 1992.

3. Rockwell, Donald, "Oscillations of Impinging Shear Layers," AIAA Journal, Vol. 21, No. 5, May 1983, pp. 645-663.

4. Whitesides, R. H., A. Gosh, S. L. Jenkins, and D. L. Bacchus, "Cold Flow Determination of the Internal Flow Environment Around the Submerged TVC Nozzle for the Space Shuttle SRM," 1989 JANNAF Propulsion Meeting, Cleveland Convention Center, Cleveland, Ohio, May 23-25, 1989.

5. Waesche, R. H. W., J. F. Marchman, and S. Kuppa, "Effects of Grain Slots on Flow in a Solid Rocket Motor," Journal of Propulsion and Power, Vol. 7, 1991.

6. Waesche, R. H. W., W. H. Sargent, and J. F. Marchman, "Space Shuttle Solid Rocket Motor Aft-End Internal Flows," Journal of Propulsion and Power, Vol. 4, 1989.

7. Desievi, F., Viguir, H.C., Greitzer, E.N., and Tan, C.S., "Mechanisms of Inlet-Vortex Formation," Journal of Fluid Mechanics, Vol. 124, pp. 173-207, 1982.